ELSEVIER

Contents lists available at ScienceDirect

# International Journal of Fatigue

journal homepage: www.elsevier.com/locate/ijfatigue





# The significance of microstructure heterogeneities on the VHCF life of cast aluminum alloys $^{\,\!\!\!\!/}$

M. Kreins <sup>a,\*</sup> , H. Kannan <sup>a</sup>, S. Scherbring <sup>b</sup>, A. Bührig-Polaczek <sup>c</sup>, J. Tenkamp <sup>d,e</sup>, F. Walther <sup>d</sup>, W. Michels <sup>b</sup>, U. Krupp <sup>a</sup>

- <sup>a</sup> IEHK Steel Institute, RWTH Aachen University, Intzestraße 1, 52072 Aachen, Germany
- <sup>b</sup> Materials Design and Structural Integrity Laboratory, Osnabrück University of Applied Sciences, 49076 Osnabrück, Germany
- <sup>c</sup> GI Foundry Institute, RWTH Aachen University, Intzestraße 5, 52072 Aachen, Germany
- d Chair of Materials Test Engineering (WPT), TU Dortmund University, Baroper Str. 303, 44227 Dortmund, Germany
- <sup>e</sup> MAN Energy Solutions, ETM Material Technology, Steinbrinkstrasse 1, 46145 Oberhausen, Germany

#### ARTICLE INFO

#### Keywords: Very high cycle fatigue Aluminum cast alloys Defect tolerance Pores SDAS

#### ABSTRACT

The very high cycle fatigue (VHCF) of cast aluminum is strongly associated with casting defects and microstructure features, e.g. porosity, (secondary) dendrite arm spacing (SDAS) and intermetallics. Complex components have an inhomogeneous microstructure due to locally varying solidification conditions. Due to complex geometries, directional solidification and sufficient feeding are often not possible, giving rise to solidification defects and shrinkage pores. These microstructural aspects influence the service life, as demonstrated by fatigue tests on automotive engine blocks and cylinder heads. However, understanding the damage process and correlating it with the microstructure is difficult due to the large number of influencing factors and their interdependencies. To this end, laboratory melts with controlled microstructure evolution were used, allowing a variation of SDAS, eutectic Si and pores under otherwise identical boundary conditions. Mechanical resonance and ultrasonic fatigue testing in combination with high-resolution microstructure analysis show a reduction in fatigue life with increasing SDAS. Main reasons are large  $\alpha$ -aluminum cells, which provide low resistance to crack propagation. The impact of pores is depending on their size, shape and location. Large fissured pores in near-surface regions act as crack initiators, whereas small spherical pores can retard crack propagation due to crack deflection and crack tip blunting.

#### 1. Introduction

Cast aluminum alloys are increasingly used for structural lightweight applications, and therefore play a key role in improving efficiency and reducing  $\mathrm{CO}_2$  emissions in automotive engineering. In the aim of reducing the specific weight, hypo-eutectic (7–11 wt% Si) cast Al alloys show a good compromise between strength and ductility (strain at fracture > 5 %) [1]. By optimized casting processes and precipitation-strengthening (0.3–0.5 wt% Mg), these alloys can be applied for high-loaded components, such as cylinder heads of internal combustion engines or transverse control arms of the chassis unit in automotive engineering. However, associated with geometry-related variations in the solidification conditions, cast microstructures are characterized by a pronounced microstructure inhomogeneity. Parameters like SDAS, size

and shape of the eutectic silicon, porosity and thin oxide films, are strongly depending on local solidification and cooling conditions as well as on the subsequent heat treatment process [2]. The size, shape and position of those microstructure components and defects have important effects on the fatigue behavior [3–5]. The resulting large variation in fatigue strength requires a rather conservative fatigue life assessment, associated with high safety margins in component design and therefore unexploited potential in terms of lightweight construction, efficiency and CO<sub>2</sub> reduction. Improving the performance of cast Al alloys requires both, a quantitative understanding of the mutually interacting microstructure parameters with respect to fatigue strength and techniques to decrease the microstructure heterogeneity. Pores, especially shrinkage pores with a cleft morphology, are very detrimental as they lead to local stress peaks that facilitate crack initiation under external cyclic loading

E-mail address: marion.kreins@iehk.rwth-aachen.de (M. Kreins).

 $<sup>^{\</sup>star}$  This article is part of a special issue entitled: 'Fatigue at VHCF9' published in International Journal of Fatigue.

<sup>\*</sup> Corresponding author.

[6,7]. Studies in the HCF regime revealed that the most detrimental influence of porosity vanishes when the size of the pores is limited to about 25 –50  $\mu$ m [8,9]. However, it is difficult to make generalized statements, as the shape of the pores (spherical vs. fissured) and the correspondingly different local stress increase also appear to have an influence [7,10]. Since a pore-free state is only possible with simple geometries that allow directional solidification and continuous feeding, knowledge about the impact of pores on fatigue strength and the possibilities of pore modification, e.g. due to gasification of the melt prior to casting, are in the focus of current research [11].

In addition to casting defects, microstructure characteristics such as SDAS, morphology and shape of eutectic silicon, inclusions and precipitates also have a significant influence on fatigue properties. The precipitates have different elastic and plastic properties than the aluminum matrix, and the strain mismatch during loading can act as an initiator for fatigue cracks [12]. In low-precipitation microstructures, deformation is mainly promoted by the formation of persistent slip bands (PSB). Precipitates might be advantageous, as they can act as a barrier for the dislocation movement, prevent pile-up and help in delaying crack initiation [13]. But while decreasing SDAS and/or precipitation strengthening increases static strength, their impact on the HCF and VHCF properties is not fully understood and currently the focus of numerous experimental and simulative analyses [4,14,15].

The purpose of this study is to investigate the microscopic and the macroscopic mechanisms involved in crack initiation and crack propagation that determine the fatigue life of cast Al-Si alloys. Therefore, the relationship between the intrinsic fatigue strength and the resistance to crack propagation (damage tolerance) of the microstructure needs to be quantified and correlated with the spatial phase and pore arrangement [13].

#### 2. Experimental

# 2.1. Materials and casting processes

Industrially produced aluminum cast components with complex geometries and consequently locally different solidification conditions serve as the starting point for fatigue testing. In order to obtain a versatile representation of the various microstructure characteristics and manufacturing defects, samples were taken from automotive engine blocks and cylinder heads at different positions within the component. The cylinder heads with a chemical composition of AlSi7Cu0.5 Mg represent a classic hypoeutectic primary metallurgy alloy, while the engine blocks from secondary metallurgy have an increased Cu content (AlSi8Cu3) and an increased proportion of Fe impurities. The samples from the engine block and cylinder head were taken at various locations with high and low cooling rates, bearing seat and stud bolt, respectively (Fig. 1), in order to represent the full range of different solidification conditions and to record variations in the resulting SDAS and pore

distribution within the component. The stud bold has a low cooling rate and consequently a slow solidification and high SDAS compared to the bearing seat and combustion chamber position.

The complex and locally varying microstructure of real components makes it difficult to systematically test individual influencing factors, which is why laboratory melts were produced under controlled solidification conditions. The aim of these was to investigate the influence of (i) eutectic Si, (ii) SDAS and (iii) pores under otherwise identical conditions.

In order to investigate the influence of SDAS on fatigue properties, the two alloys of the engine block and cylinder head (AlSi8Cu3 and AlSi7Cu0.5 Mg) were cast in a specially developed stepped wedge on a laboratory scale (Fig. 2). The stepped wedge shape enables different cooling rates depending on the thickness of the step in a single casting. Consequently, the SDAS can be precisely varied under otherwise identical microstructure characteristics. The laboratory casting process involved melting the alloy at 750  $^{\circ}$ C in an induction furnace and casting into steel molds preheated to 730  $^{\circ}$ C. To enhance grain refinement and eutectic silicon modification, AlTi5B1 (grain refiner) and AlSr10 (modifier) were added prior to casting.

For the aim of pore analysis, selected samples from the industrial components and the laboratory melts were hot isostatically pressed (HIP) in order to obtain an almost pore-free reference condition. HIP was carried out at approx. 70 % of the melting temperature and a pressure >75 MPa using the patented Densal<sup>TM</sup> process. Additionally, the influence of pore amount, size and morphology was studied based on lab castings to modify pore characteristics. Cylindrical rods were cast using gravity die casting with a pneumatic activation of the casting process and optimized filling conditions to control temperature and reduce meltair contact time (Fig. 3), cf. [11]. Based on extensive preliminary work, the industrially well-established alloy AlSi11Mg0.2 was selected as an example. As expected, shrinkage pores form in the upper sample area. To avoid this, pores were modified by gasifying the melt prior to casting with a gas mixture consisting of 30 vol% hydrogen and 70 vol% argon using a rotary impeller (IDECO GmbH) at a speed of 500 rpm. This makes it possible to replace the large, fissured shrinkage pores by small, spherical hydrogen pores. Details on the casting system, resulting solidification conditions as well as the hydrogen gasification process can be found in previous publications [11].

#### 2.2. Microstructure characterization

Industrial components as well as lab castings were subjected to metallographic analysis to determine SDAS, as well as size and shape of eutectic Si and porosity. Samples for microstructural characterization were cold-embedded, ground, and polished to a grit size of  $0.3~\mu m$  using colloidal SiO<sub>2</sub> polishing suspension (OPS). To ensure comparability of the samples and extraction sites individually and with each other, the SDAS was determined according to BDG guideline P220 [17] using the

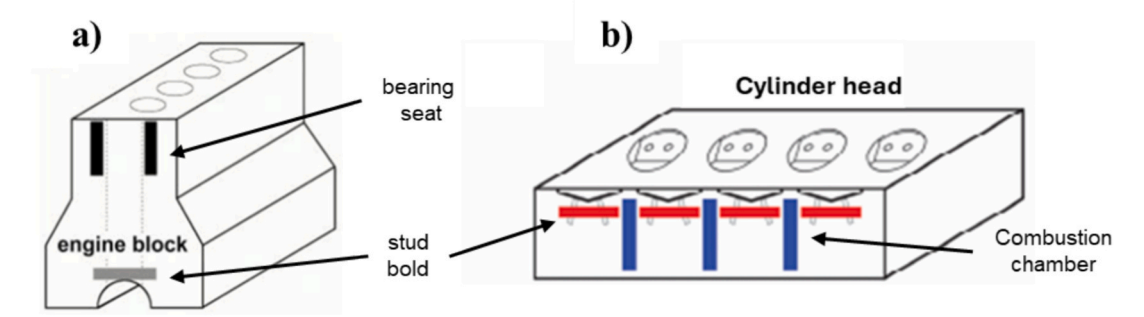


**Fig. 1.** In-series sand cast engine block (AlSi8Cu3) with positions of specimen extraction marked in black for the bearing seat (high cooling rate, low SDAS) and grey for the stud bold (low cooling rate, high SDAS); b) cylinder head (AlSi7Cu0.5 Mg) with stud bold position (low cooling rate, high SDAS) in red and combustion chamber (high cooling rate, low SDAS) in blue. [13,16].

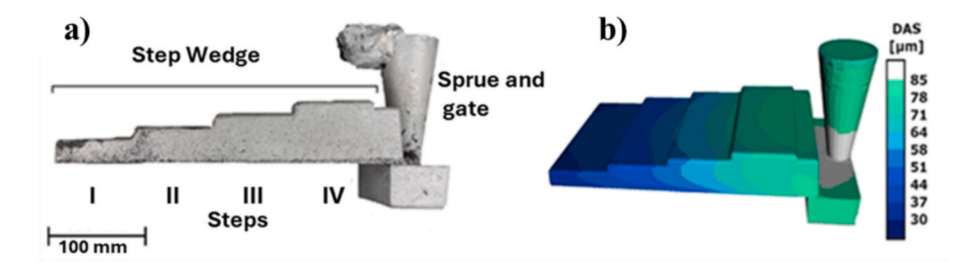


Fig. 2. Step wedge developed to vary the solidification rate a) Casting of the Al-Si8Cu3 alloy and b) Results of the solidification simulation showing the variation of DAS in the steps.

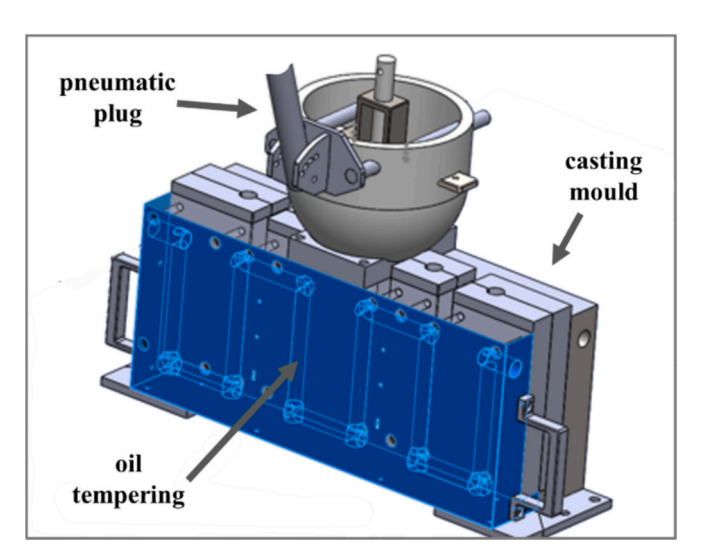


Fig. 3. Gravity die casting with a pneumatic activation of the casting process and optimized filling conditions to control temperature and reduce melt-air contact time [11].

line cut method with a minimum of five SDAS.

Porosity was quantified by light optical microscopy (LOM) and by non-destructive X-ray computer tomography (Procon  $\mu$ CT) prior to fatigue testing to obtain porosity information on the complete volume of the sample. Based on the 3D data, pores were automatically identified and analyzed regarding size and shape by applying a deep learning method implemented in the software "Dragonfly" (Object Research Systems). This method was also used to visualize not only the pores but also the 3D crack profile of crack propagation tests. Additionally, high-resolution scanning electron microscopy (SEM, Zeiss Auriga FEG), combined with electron backscatter diffraction (EBSD) and energy-dispersive X-ray spectroscopy (EDS) was used to analyze the crack surface and correlate the crack paths to microstructural characteristics and crystallographic orientations.

## 2.3. Fatigue testing

The dependency of fatigue life on microstructural features, such as porosity, SDAS and size of eutectic Si, is studied using a 1000 Hz resonance testing machine (Gigaforte 50, Rumul), a 20 kHz ultrasonic testing machine (UFTE type BOKU Vienna), a 90 Hz resonance testing maschine (Testronic, Rumul), and by crack propagation tests using 100 Hz resonance bending device (Cracktronic, Rumul).

Resonance fatigue testing at 1000 Hz was performed at stress amplitudes between 70 and 100 MPa and a stress ratio of R=-1. The tests were carried out on cylindrical specimens (diameter: 7 mm diameter, parallel length: 11 mm) according to ISO 1099 [18] and DIN 50100 [19], that were polished prior to testing in order to avoid surface effects due to machining.

Ultrasonic fatigue testing at  $f\approx 20.0\pm 0.2$  kHz and R=-1 (testing using UFTE type BOKU Vienna) was performed in pulse-pause mode (20:80) using a pneumatic air-cooling system in order to avoid temperature increase during testing. The specimen geometry is schematically shown in Fig. 4a. Due to the very high effort involved in sample preparation and the long test duration, the Hück stair tread method [20] was used to determine the conditional fatigue strength  $\sigma_f$  at  $N_f=10^9$  cycles.

In-situ crack monitoring was conducted during resonance fatigue testing at approximately 90 Hz (Rumul Testronic). The tests were carried out on cylindrical specimens with the same geometry as the 1000 Hz testing (diameter: 7 mm diameter, parallel length: 11 mm). For crack growth analysis, trigger signal was sent to a Hirox MXB-10c digital microscope after every 50 cycles at maximum applied load. This enabled the acquisition of images of a polished, shallow notch on the specimen surface.

Crack propagation behavior was studied by bending resonance frequency testing at 100 Hz and R =-1 (Rumul Cracktronic) using single-edge notched bend (SENB) samples (Fig. 4b) according to ASTM E647 [21]. Initially, a pre-cracking step is performed to obtain a sharpened straight fatigue crack of 1.3 mm length. Crack propagation tests were performed using the load shedding technique since the near-threshold data is required. In this test, a constant R value of -1 is maintained while  $\Delta K$  is reduced gradually until the crack growth becomes technically irrelevant (less than  $10^{-10}$  m/load cycle). Subsequently, the constant load amplitude test procedure is performed to obtain higher crack growth rates and to determine the parameters of the Paris crack propagation law [21].

The rate of crack growth  $\left(\frac{dA}{dN}\right)$  is obtained by Eq. (1) where C and m are constants obtained from the crack propagation tests [22]. The operating stress intensity factor range  $\Delta K$  during crack propagation tests is calculated according to Eq. (2) with the nominal bending stress range  $\Delta \sigma_b$ , the crack length a and the geometry factor Y(a/w) for SENB specimens, which is dependent on crack length and width of the specimen (cf. Fig. 4) [23,24].

$$\frac{dA}{dN} = c \bullet \Delta K^m \tag{1}$$

$$\Delta K = \Delta \sigma_b \sqrt{\pi a} \bullet Y \left(\frac{a}{w}\right)$$
with  $Y = \sqrt{\frac{2W}{\pi a} tan\left(\frac{\pi a}{2W}\right)} \left(\frac{0.923 + 0.199\left(1 - sin\left(\frac{\pi a}{2W}\right)\right)^4}{cos\left(\frac{\pi a}{2W}\right)}\right)$  (2)

According to ASTM E647, the threshold value  $\Delta K_{th}$  can be determined if at least five data points are available for the crack growth rate in the range of  $10^{-10}$  m/cycle < da/dN <  $10^{-9}$  m/cycle. Using these data points, a best-fit line for  $\Delta K$  versus da/dN is calculated and extrapolated to da/dN =  $10^{-10}$  m/cycle. The corresponding stress intensity factor (SIF) range  $\Delta K$  at this point is considered the threshold  $\Delta K_{th}$ .

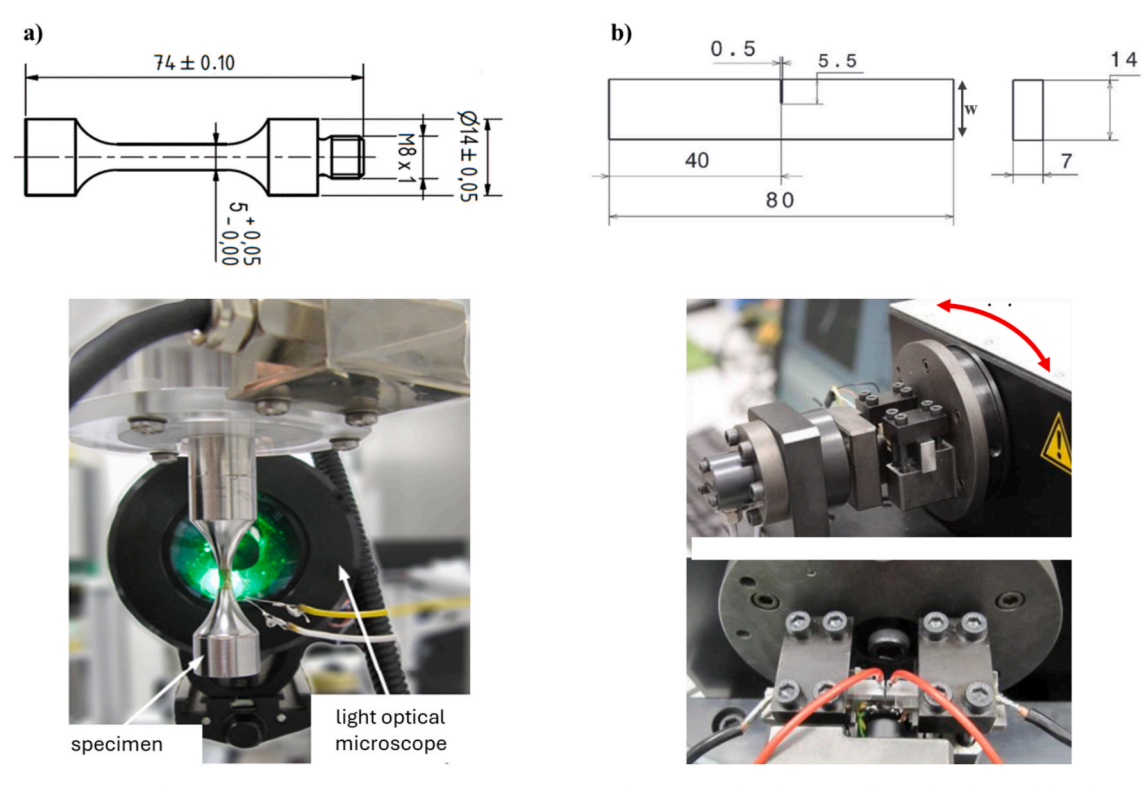


Fig. 4. Sample geometry in mm for a) VHCF testing using UFTE type BOKU Vienna, 20 kHz equipped with LOM and b) single edge notch bend (SENB) specimen for crack propagation testing using Rumul cracktronic.

#### 3. Results and discussion

# 3.1. Fatigue strength of industrial cast engine block and cylinder head

The fatigue experiments on industrially manufactured components have revealed major differences in service life, not only between different components, but also within a single component. First of all, it can be stated that the cylinder head made of primary aluminium (AlSi7Cu0.5 Mg) generally shows a higher conditional fatigue strength (fatigue strength corresponding to the fatigue life  $N_f=10^9\,\mbox{cycles})$  than the engine block made of secondary alloy (AlSi8Cu3). As shown in Fig. 5a, the conditional fatigue strength  $\sigma_{10^9}$  reaches a maximum of 101 MPa in the bearing seat of the engine block and 122 MPa in the combustion chamber side of the cylinder head. This difference in fatigue strength is superimposed by local variations within the component, which is 30 MPa in both the cylinder head and the engine block. The bearing seat has a significantly lower conditional fatigue strength of  $\sigma_{10^9}$ = 68 MPa in the engine block and  $\sigma_{10^9}=$  90 MPa in the cylinder head for both components. Finally, it should be noted that the fatigue tests on one and the same component position also show an enormous scatter, with up to  $\pm 23$  MPa for the bearing seat of the engine block.

Reason for the enormous differences in the fatigue strength are differences in the microstructure, i.e., local and global inhomogeneities, which also explains the scatter in service life. Firstly, the microstructure is determined by the chemical composition (primary vs. secondary aluminium) and the associated phases and precipitations. Secondly, the solidification conditions, depending on the local cooling rate in the component, are decisive for numerous microstructure characteristics such as SDAS, proportion and morphology of the eutectic Si and intermetallic phases, porosity and pore morphology.

Analysing the microstructure of the engine block and cylinder head at the various locations has revealed massive differences in the microstructure characteristics listed above, some of which show a clear correlation with fatigue strength. The differences in SDAS are particularly striking, whereby a higher SDAS correlates with a poorer fatigue strength (Fig. 5b). Due to the lowest cooling rate, the engine block stud bolt has the highest SDAS of 65  $\mu m$  and a pronounced scatter of  $\pm 10~\mu m$ , which apparently contributes to the poor fatigue strength of  $\sigma_{10^9}=68$  MPa. The massive differences in SDAS between engine block stud bolt and bearing seat can be clearly seen in the light optical microscopy images in Fig. 6. As expected, low cooling rates result in a coarse microstructure large  $\alpha$  Al cells, whereas high cooling rates promote low SDAS and finely distributed  $\alpha$ -Al cells.

In addition to the SDAS, porosity and the average pore diameter also appear to have a massive influence on the fatigue strength. The engine block stud bolt, with the lowest fatigue strength, also shows a factor of 10 higher porosity and a factor of 5 larger average pore diameter compared to the other samples (Fig. 5d). This is not surprising, as it is generally known that pores can lead to local stress concentration and favour crack initiation.

However, the influence of pores is also superimposed by the influence of eutectic Si. The engine block stud bolt also has by far the lowest shape factor of the eutectic Si, i.e., the Si is more needle or plate-like but not round in shape (Fig. 5c). A closer analysis of the microstructure shows that the Si in the stud bolt is locally very inhomogeneous, resulting in a bimodal distribution (Fig. 7a). Some areas show small round-shaped Si particles, whereas other areas show large, needle-shaped Si particles. The eutectic Si in the bearing seat, on the other hand, is significantly smaller and more rounded in all areas (Fig. 7b). Since the different elastic plastic properties of Si and the surrounding matrix lead to stress fields that interact with the crack tip, an influence on the fatigue strength is also to be expected.

Since the influence of the previously identified factors (i) SDAS, (ii) porosity and pore size and (iii) Si size and shape are superimposed, it is uncertain which of the factors is the decisive one for the fatigue strength or to what extent the respective factors influence the service life. Since all of those microstructural features are influenced by the cooling rate and thus solidification conditions, they are mutually dependent. A comprehensive analysis of various samples from the cylinder head and the stepped wedge samples shows the general correlation that an

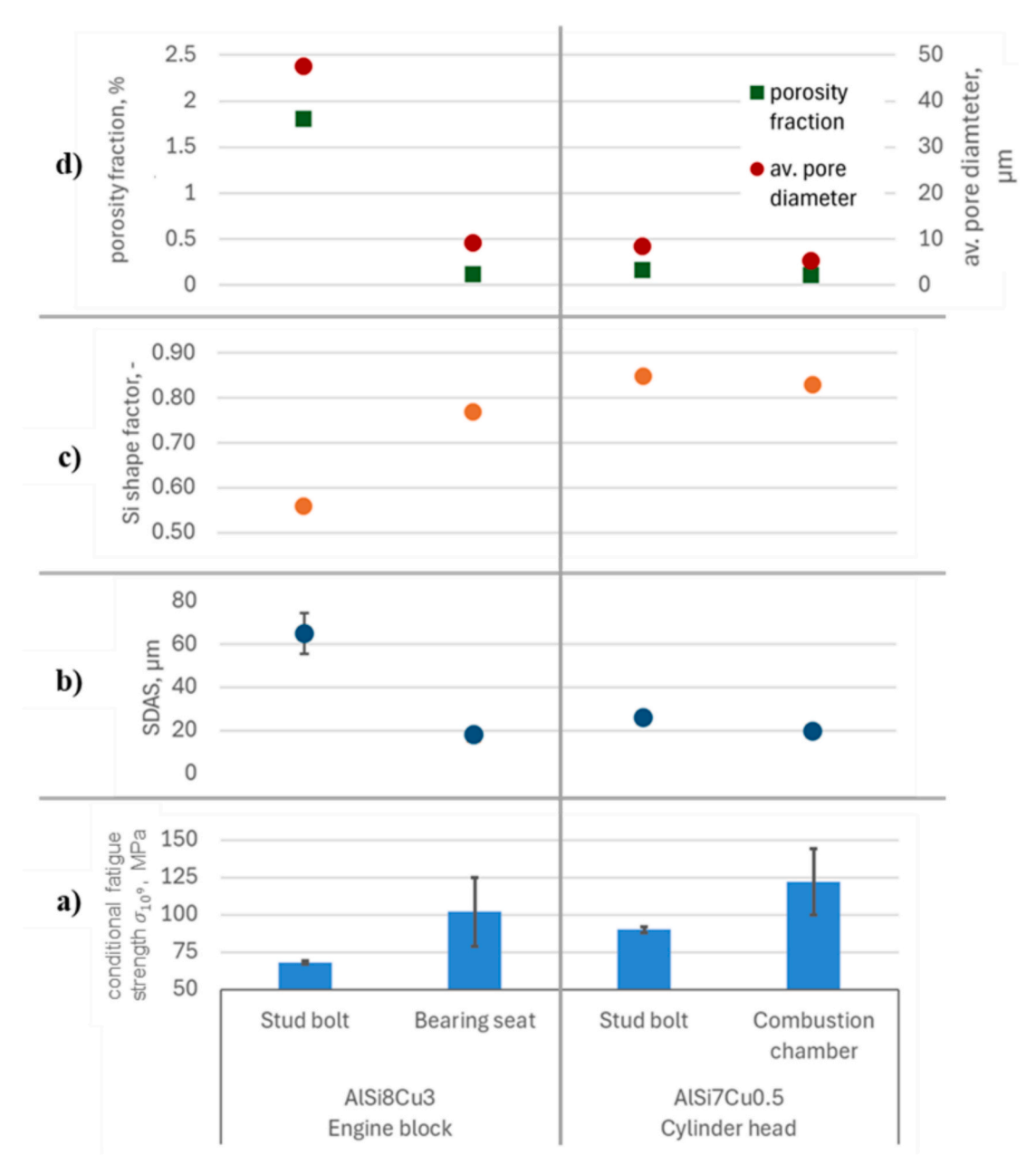


Fig. 5. Microstructure of the engine block and cylinder head at different sample positions with high cooling rate (bearing seat and combustion chamber) and low cooling rate (stud bolt); a) conditional fatigue strength  $\sigma_f$  at  $N_f=10^9$  cycles, obtained by ultrasonic fatigue testing at 20 kHz and R=-1 (UFTE, Boku Vienna), b) SDAS, c) average shape factor (SF) of eutectic Si ( $SF=4\pi A/P^2$  with A= area and P= perimeter of the particle; SF=1 corresponds to a circle), d) porosity fraction and average pore diameter.

increasing cooling rate decreases SDAS, reduces the pore diameter and results in rounder pores. This applies not only to the pores, but also to the size and shape of the Si particles (Fig. 8). It is therefore not possible to analyse the influence of individual microstructure parameters on the fatigue properties of a real component isolated from others. However, knowledge and understanding of these correlations is of great importance for component design and material optimisation. Therefore, the influence of selected parameters has been analysed in more detail using laboratory melts produced under controlled and homogeneous solidification conditions.

#### 3.2. Influence of eutectic Si and intermetallics on fatigue strength

Eutectic Si particles and intermetallic phases lead to local stress inhomogeneities in the microstructure, which can have a massive

influence on crack initiation and crack growth. Their amount, size and morphology are particularly important and significantly influenced by the local temperature profile and heat treatment condition. Fig. 9 shows the microstructure in the as-cast condition and after T6 heat treatment (solution treated at 540  $^{\circ}\text{C}$  for 1 h, water quenching and artificial aging at 170  $^{\circ}\text{C}$  for 8 h) as an example for the wedge cast AlSi7Mg0.3.

The as-cast microstructure primarily comprises the aluminum matrix ( $\alpha$  phase), eutectic silicon (Si), and intermetallic phases. According to literature, the intermetallics present in these alloys were mainly acciular or plate-shaped  $\beta$ -Al $_5$ FeSi phase and the Chinese script  $\pi$ -Al $_8$ FeMg $_3$ Si $_6$  phase [21]. It is well known that these phases act as stress concentrator, which is why grain refiners like Sc are added in order to promote the formation of intermetallic of globular morphology to improve mechanical properties [25]. The formation and growth of primary Mg $_2$ Si, which is mainly responsible for precipitation hardening in Al-Mg-Si

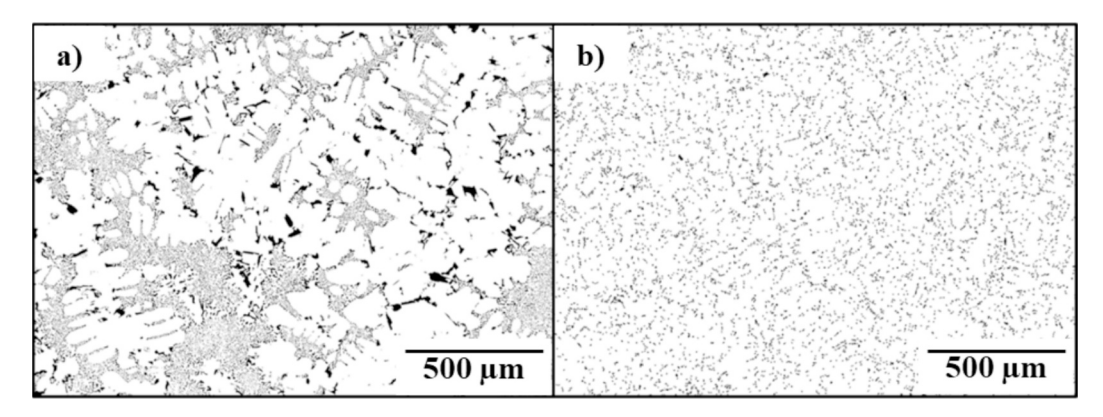


Fig. 6. Representation of the eutectic silicon of alloy AlSi8Cu3 with a) stud bolt SDAS = 65 µm and b) bearing seat SDAS = 18 µm.

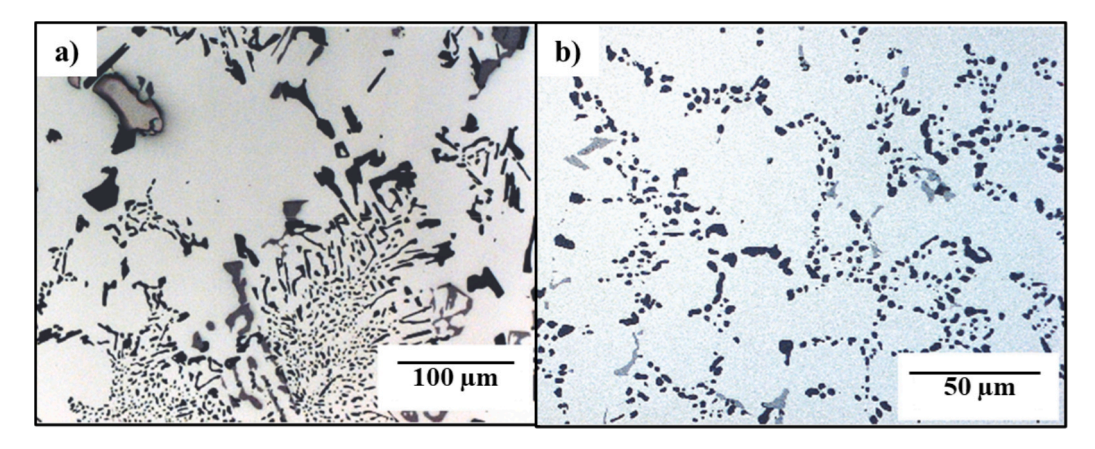


Fig. 7. Microstructure of AlSi8Cu3 engine block, showing a) bimodal distribution of eutectic Si in the stud bolt and b) smaller and more spherical Si in the bearing seat.

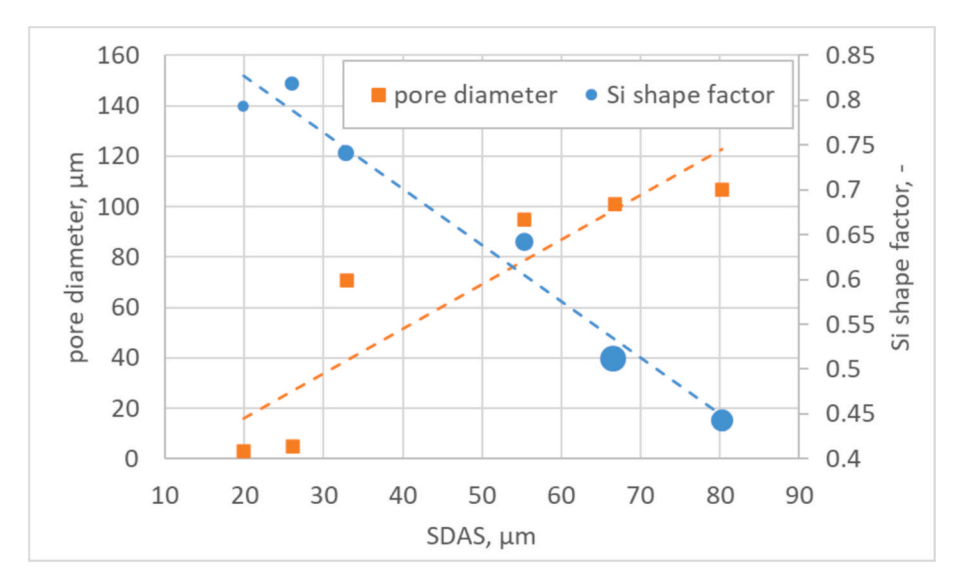


Fig. 8. Dependence of the Si size and pore diameter depending on the SDAS for AlSi7Mg0.3 and AlSi7Cu0.5 Mg. The average size of Si particles is qualitatively represented by the size of the blue circles (Si shape factor).

alloys [26], were found to occur heterogeneously on oxide inclusion surfaces, such as alumina or spinel particles in magnesium-rich compositions. This aligns with the multistep nucleation hypothesis, which suggests that primary intermetallic phases nucleate on oxide particles, followed by the nucleation of primary  $\alpha$ -Al or eutectic phases [27]. During the solution treating step, the Mg<sub>2</sub>Si dissolves back into

aluminum solid solution. Then, the ageing process leads to the precipitation of Mg<sub>2</sub>Si phase which is evenly distributed in the Al matrix and leads to strengthening, i.e., an increase form 108 HV0.25 (500 °C 8 h / 160 °C 5 h) to 133 HV0.25 (545 °C 1 h / 160 °C 5 h).

Morphological changes in the microstructure were observed after the T6 heat treatment. In particular, the irregular eutectic Si phase present

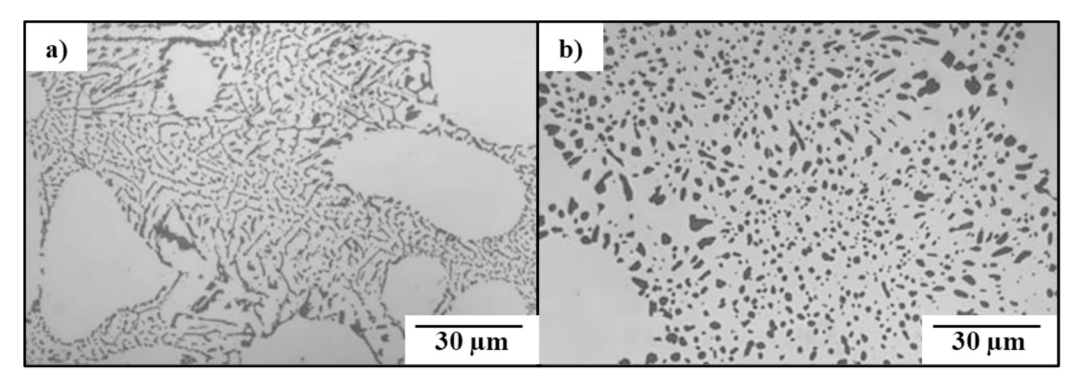


Fig. 9. Shape of eutectic silicon of the wedge cast AlSi7Mg0.3 alloy a) before and b) after T6 treatment.

in the as-cast condition was transformed into fine spheroidized particles uniformly distributed within the aluminum matrix. In the as-cast samples, the eutectic Si particles exhibited a needle-like morphology, which is known to act as stress concentrators, thereby facilitating the initiation of fatigue cracks under cyclic loading conditions. However, post-T6 treatment, these Si particles underwent a morphological transformation as shown in Fig. 10, becoming round and significantly reducing their stress-raising effect. Therefore an increase in fatigue life can be achieved by finely distributed and spherically molded Si precipitates in a precipitation-hardened aluminum matrix [28].

The local interaction of the crack tip with microstructural features was analyzed in more detail by in situ observation of crack growth by light optical microscope (LOM). As it can be seen in Fig. 11, the eutectic Si has a significant influence on the local crack propagation rate. Cracks tend to propagate in a relatively straight line in single-phase dendritic FCC Al (green arrows in Fig. 11b), while while in areas of interdendritic eutectic Si they often change direction and show many kinks (orange arrows in Fig. 11b). Throughout the large eutectic interdendritic cells, the crack propagation rate is therefore lower. In contrast, crack growth is significantly promoted when the crack passes through  $\alpha$ -aluminum dendritic cells.

The analysis of the crack propagation using EBSD on the polished surface of an SENB specimen (100 Hz resonance bending), exemplarily shown in Fig. 12 for the cylinder head stud bolt, shows a strong interaction of the crack with the local microstructure. Based on the Euler angles, the {111} slip planes were calculated and displayed for the 3 largest grains via the slip plane projections in the circles (Fig. 12a). It can be clearly seen that cracks tend to propagate along the {111} slip planes of the single-phase dendritic FCC Al. Even if there is crack splitting (e.g. in blue grain no. 1), the individual partial cracks run along different {111} planes until a recombination of the crack finally occurs. The frequent crack splitting and recombination as well as the jagged course of the crack due to the inhomogeneous microstructure can be seen particularly well on the image quality map (Fig. 12b).

#### 3.3. Influence of SDAS on fatigue strength

The influence of the SDAS on the fatigue strength was already evident from the engine block and cylinder head samples analysed above, but the influence could not be investigated in isolation due to simultaneous changes in porosity. For this purpose, a specific analysis of the impact of SDAS on fatigue life has been carried out using step-wedge laboratory samples, which, due to the different thickness of the step, allow a precise variation of the cooling rate and thus the SDAS under otherwise almost identical conditions. The results of the corresponding VHCF experiments in Fig. 12 clearly show that the fatigue strength  $\sigma_{10^9}$ significantly decreases with increasing SDAS for both alloys. The corresponding trend curves show a decrease of 0.34 and 0.46 MPa per µm SDAS for the cylinder head and the engine block respectively. This correlation between SDAS and cyclic strength complements well with the correlations between SDAS and quasi-static strength discussed in the literature. Yajjala et al. [29] report a decrease in yield strength (YS) of 0.797 MPa per µm SDAS and ultimate tensile strength (UTS) of 1.707 MPa per  $\mu$ m SDAS for cast A356 alloy in the T6 heat-treated condition. In contrast, Yan et al. correlate YS via the square root of SDAS analogue to the Hall Petch relation and obtain a good agreement (goodness of fit R<sup>2</sup> = 0.920) with a Hall Petch constant K of 195.64 [30]. A Hall Petch correlation between grain size and fatigue strength has already been demonstrated for various steels. Chapetti et al. show a good correlation with a Hall Petch constant K of 300 based on experiments on ultra-fine grained steels and literature data on ferritic-pearlitic and ultra low carbon steels [31]. This is in good agreement with the observations in this study, but with the crucial difference that the decisive microstructure parameter for Al casting alloys is not the grain size, but the SDAS. The great importance of SDAS for the cyclic properties of Al cast alloys is also confirmed by the latest analyses by Lang et al. on an A356-T6 alloy, which show an inverse relationship between SDAS and fatigue limit both experimentally and simulatively [32].

The conditional fatigue strength of  $\sigma_{10^9}$  of the engine block and the

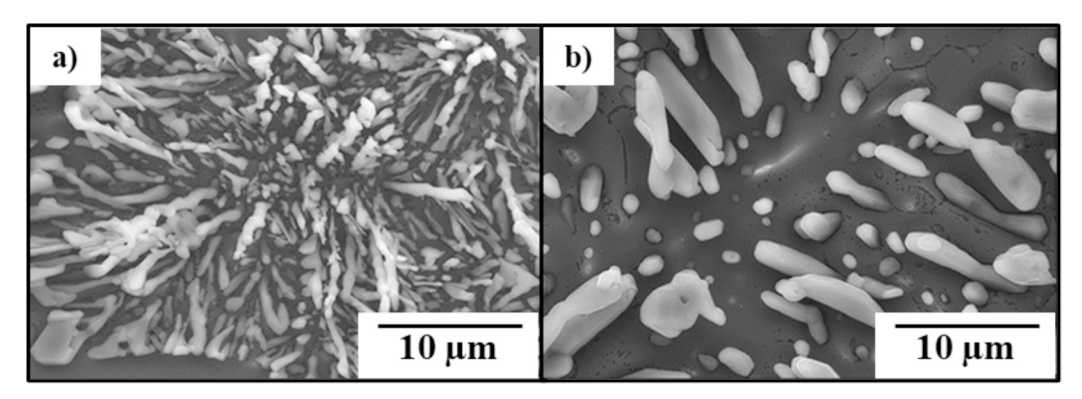


Fig. 10. Morphological change of silicon of the wedge cast AlSi7Mg0.3 alloy from a) before (as cast) and b) after solution treatment at 540 °C for 1 h [2].

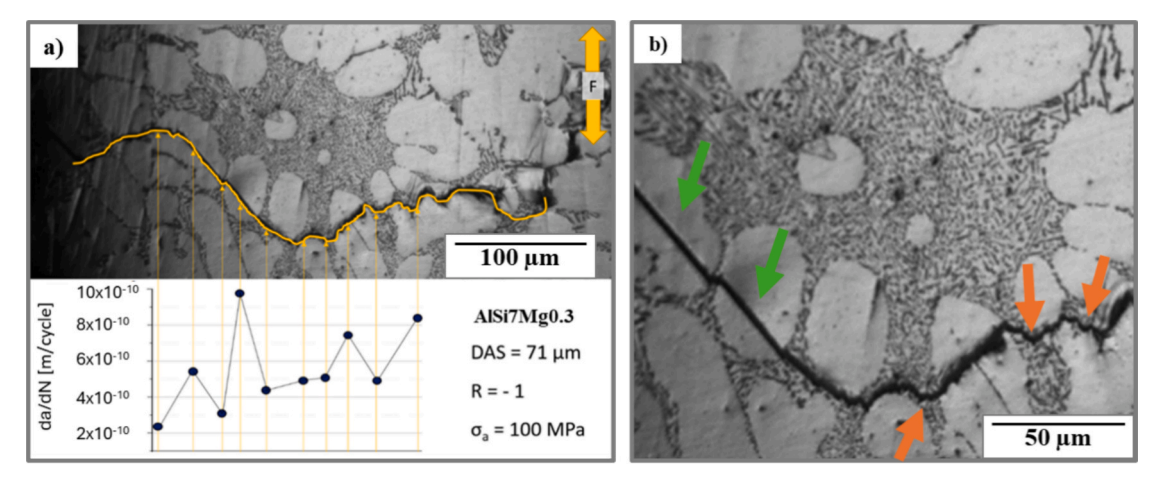


Fig. 11. a) Influence of the microstructure on the crack propagation rate da/dN for wedge cast AlSi7Mg0.3 alloy, tested at R = -1,  $\sigma_a = 100$  MPa and f = 90 Hz (Rumul Testronic). Crack propagation rate da/dn was determined based on a Matelect ACPD crack length measurement system (cf. [13].). b) Enlarged image from a), demonstrating that the crack propagates in a relatively straight line in single-phase dendritic FCC Al (green arrows), while it shows many kinks in interdendritic eutectic Si (orange arrows).

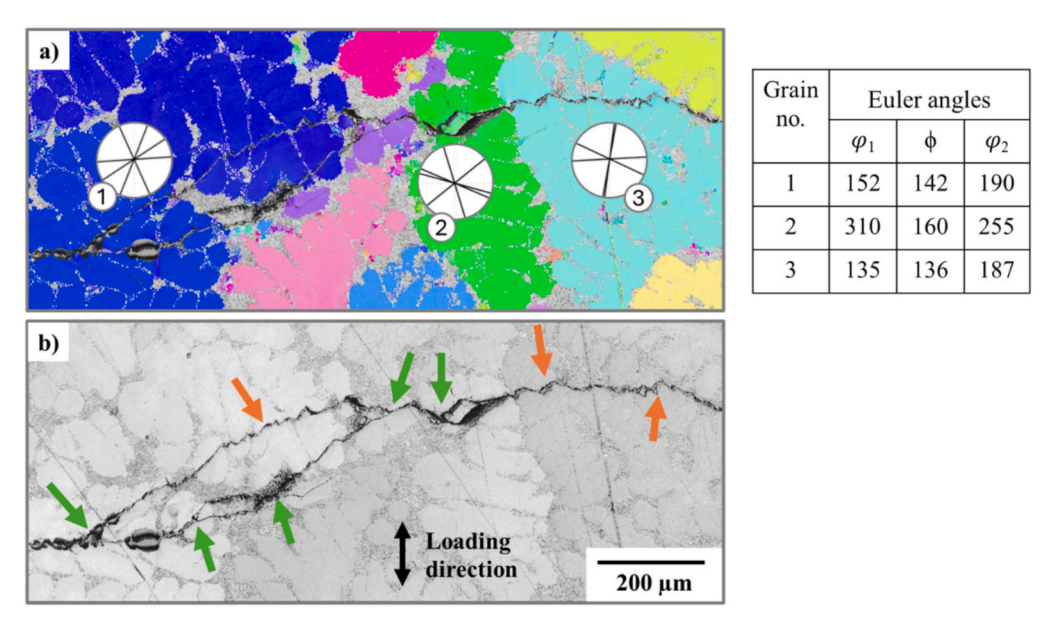


Fig. 12. EBSD data recorded on the polished surface of a SENB sample (100 Hz resonance bending) from the cylinder head stud bolt. a) IPF Map with grain orientation shown by colour. The crack often propagates along the {111} slip planes, which were calculated based on Euler angles and indicated in orientation circles for three selected grains. b) Image quality map clearly shows the jagged crack pattern due to the inhomogeneous microstructure (orange arrows) as well as multiple splitting and recombining of the crack (green arrows).

cylinder head is shown as orange circles in Fig. 12, corresponding to the SDAS. In general, the data points of the industrial component show a similar progression to the laboratory melts, but are at different levels and show a significant scatter. Industrial components are optimized for efficiency. This often results in variations in microstructure across different sections of the component. For instance, in an engine block, areas experiencing low stress may exhibit a less refined microstructure compared to the cylinder head. The exceptionally good fatigue strength of the cylinder head combustion chamber with very low SDAS is striking. In the engine block, on the other hand, the fatigue strength of the bearing seat (SDAS = 65  $\mu m$ ) at only 65 MPa is significantly lower than that of the laboratory melt at 80 MPa. The reason for this is seen in the fact that with the high SDAS in the industrial component, the porosity also increases significantly, as discussed in more detail in section 3.4.

The influence of the SDAS on crack growth was analysed using crack propagation curves from resonance bending tests, as shown in Fig. 13. Using the example of wedge cast AlSi8Cu3, it becomes very clear that

the threshold value of the stress intensity factor  $\Delta K_{th}$  decreases with decreasing SDAS. By regression analysis, a formal relationship between the SDAS and the threshold value against technical crack initiation can be established. The results based on crack propagation experiments on step wedge samples are summarized in Fig. 14, where the threshold value  $\Delta K_{th}$  is plotted over the reciprocal square root of the SDAS (in analogy to the Hall-Petch relationship). However, unlike the fundamental relationship according to Hall and Pech, the threshold decreases with decreasing SDAS. This observation is surprising at first, as a finer microstructure (small grain size or SDAS) generally shows more obstacles for dislocation slip and microstructural short-crack growth, and can therefore generally be expected to have better mechanical properties. In addition, the ultrasonic fatigue tests previously discussed (Fig. 12) have shown that a low SDAS leads to a higher fatigue strength. However, it should be noted that the crack initiation phase is particularly important for the latter. A low SDAS appears to have a positive effect here, whereas a high SDAS appears to be favorable regarding the threshold against

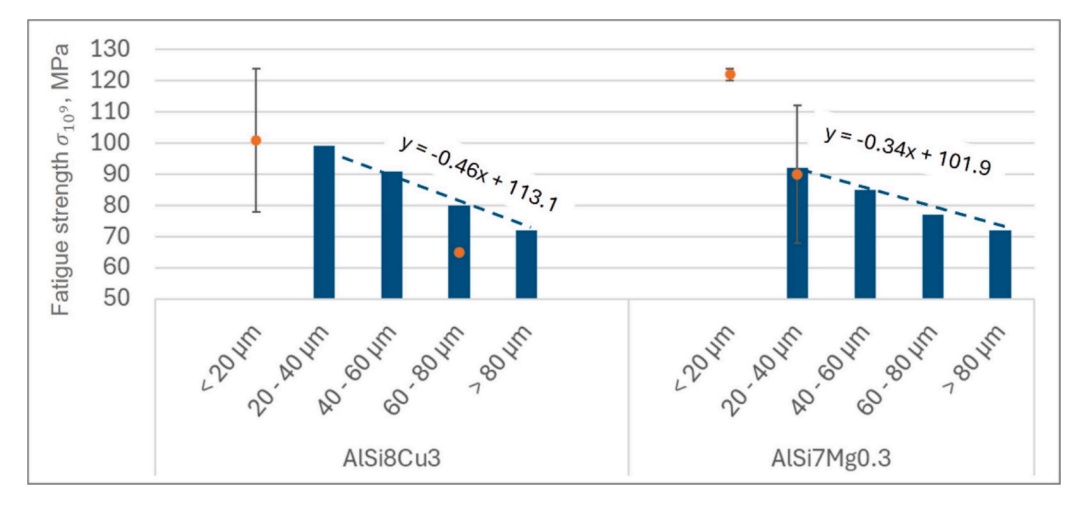


Fig. 13. Conditional fatigue strength  $\sigma_{10^9}$  of step wedge samples with different SDAS. Additionally, conditional fatigue strength  $\sigma_{10^9}$  of industrial cast engine block (AlSi8Cu3) and the cylinder head (AlSi7Mg0.5) specimens is shown as orange circles according to their SDAS (ultrasonic fatigue testing at 20 kHz and R = -1, testing device UFTE from Boku Vienna).

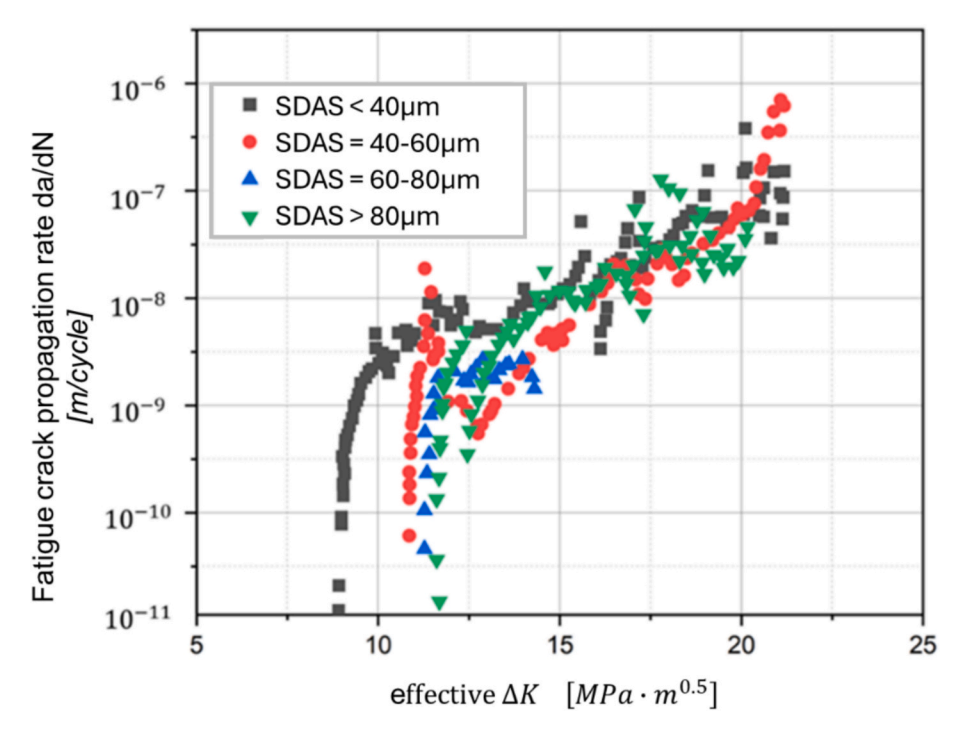


Fig. 14. Crack progression rate da/dN as a function of the effective  $\Delta K$  (stress intensity factor amplitude for R=-1) for the step wedge AlSi8Cu3 for different SDAS (bending resonance frequency testing at 100 Hz using single-edge notched bend (SENB) samples, R=-1)

propagation of an existing crack, as is the case for crack propagation tests (Fig. 14). This could be due to the fact that a higher SDAS leads to a higher roughness in the crack flank, which can favor crack closure effects. The crack path is largely determined by  $\alpha\text{-}Aluminium$  dendritic cells, the interdendritic eutectic cells and their interfaces. Cracks tend to propagate along {111} slip planes in  $\alpha\text{-}Aluminium$  dendritic cells, while they are deflected by interdendritic eutectic Si (Fig. 11). A higher SDAS leads to larger  $\alpha\text{-}Aluminium$  dendritic cells and higher distances between interdendritic eutectic Si, which consequently results in a more pronounced roughness of the crack flanks. This favors roughness-induced crack closure and can thus explain the higher threshold value against technical crack growth for large SDAS. The results are in good agreement with observations on A356 (7 % Si). The alloy also exhibits better near-threshold crack growth resistance for higher SDAS, which the authors explain by higher roughness-induced crack closure effects

[33].

The results for the industrially manufactured series component samples are shown in Fig. 14 as blue points for comparison. The bearing seat position with a low SDAS of 18  $\mu m$  fits well on the trend line. However, with a  $\Delta K_{th}$  of only 7.0  $MPa\sqrt{m}$ , the stud bold with high SDAS performs significantly worse than expected. The statistical and locally inhomogeneous distribution of Si cells and impurities such as intermetallics may be the reasons. In addition, a high SDAS and an increased proportion of pores due to a lower cooling rate can also influence crack growth. The influence of pores on fatigue strength and microstructural short crack growth is addressed in more detail in the following section.

#### 3.4. Influence of pores on fatigue strength

In order to specifically analyse the influence of pores, selected samples of the engine block and cylinder head were subjected to HIP treatment at 70 %. The combination of high temperatures (approx. 70 % of melting temperature) and pressure closes casting-related pores without affecting the SDAS, silicon morphology and intermetallics, so that the influence of pores can be analysed in isolation.

The pore analysis previously discussed showed that the pores and other volume defects are inhomogeneously distributed within the engine block and cylinder head, with a small SDAS correlating with a lower amount of more spherical pores (Fig. 8). It was clear to see that the AlSi8Cu3 engine block stud bold with large SDAS and consequently high porosity showed by far the lowest fatigue strength (Fig. 15). The high porosity is attributed to the combination of slow solidification and the negative influence of the accompanying elements in the secondary aluminium. The presence of iron bearing Al(Mn,Fe)Si intermetallic phases such as β-Al5FeSi affect the porosity, especially in secondary alloys where impurities such as Fe, Mn, Cu are present. These plateshaped intermetallics block the liquid metal from filling spaces during casting and lead to porosity. This was confirmed by Moustafa et al. [34], when they detected a higher amount of  $\beta$ -Fe platelets near the shrinkage pores. The large, fissured shrinkage pores lead to excessive localised stresses and cause crack initiation and a reduced fatigue strength, particularly in the near-surface area. HIP was able to close the pores and reduce the influence, which is reflected in a significant improvement in the conditional fatigue strength from  $\sigma_{10^9} = 68$  to  $\sigma_{10^9} = 97$  MPa AlSi8Cu3 engine block stud bold (Fig. 15). Individual samples showed no failure even after  $N_f = 10^{10}$  cycles. Other sampling positions on the engine block and cylinder head also show a significant improvement due to HIP treatment, although the effect is not quite as pronounced. Only the cylinder head stud bold is an exception here, although this is within the scattering range.

Crack propagation experiments (Fig. 16) confirm that the

elimination of pores by HIP also has a positive effect on the threshold value for technical crack growth  $\Delta K_{th}.$  The effect is very pronounced for the cylinder head stud bolt with higher SDAS and consequently larger pores. The combustion chamber with lower SDAS and correspondingly smaller pores shows no significant influence of the HIP on  $\Delta K_{th}.$ 

In order to investigate the influence of pores on the failure mechanism in more detail, selected post-fatigue fracture surfaces were analysed using scanning electron microscopy. Fig. 17 shows an example of wedge cast AlSi7Mg0.3 for two different SDAS, revealing an intriguing observation: the coexistence of both pores and facets on certain fracture surfaces. This finding contradicts the observations of Nyahumwa et al. [35], who reported that facets only occur in the absence of pores. According to Wang et al [36] and Siegfanz et al. [2] the facets are the {111} planes of the dendritic aluminium solid solution.

Fig. 18 shows a facet fracture surface with oxide inclusions. This observation supports Campbell's, albeit somewhat controversial theory of oxide films, so-called bifilms [37]. The presence of oxide inclusions and facet fracture surfaces in both un-HIPed and HIPed states suggests that these features are oxide films rather than closed pores. The presence of oxides suggests a lack of metal to metal contact. The inner sides of the bifilm do not bond together and there exists a gap between them. These dry sides of a double oxide film in cast aluminium alloys constitute a crack. Campbell described that during solidification of casting, the entrained bifilm may straighten or unfurled and mechanically flattened by the growth of dendrites.

The outer surface of bifilm is in perfect atomic contact with the matrix and the only solid surface available at an early stage of cooling of the liquid. Therefore, they are probably favored substrates for the precipitation of second phases as intermetallic compounds. Because the intermetallic compound usually grows on either side of the bifilm, the central unbonded interface of the bifilm often appears as a crack along the center of the growing particle. The crack-like nature of bifilms suspended in aluminum alloy castings leads to premature failures and thus reduces the mechanical properties of castings [29].

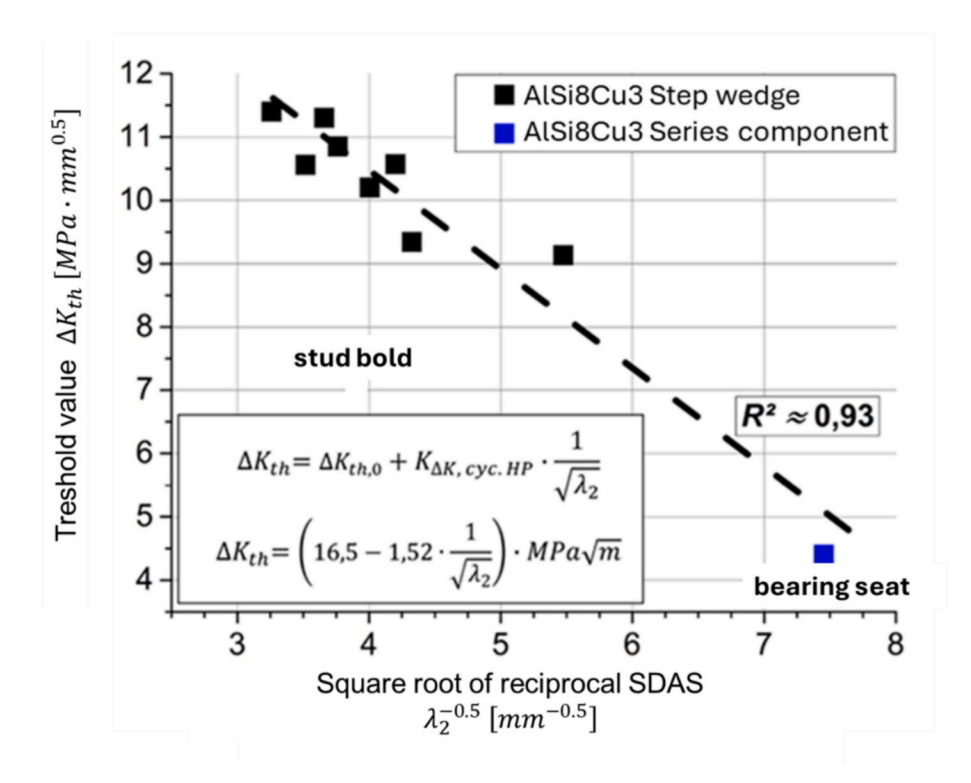


Fig. 15. Representation of the alternating deformation tests on AlSi8Cu3 step wedge specimens (black) and series components (blue); in analogy to the Hall-Petch relationship, a good correlation between  $\Delta K_{th}$  and the root of the reciprocal SDAS is shown SDAS (bending resonance frequency testing at 100 Hz using single-edge notched bend (SENB) samples, R = -1).

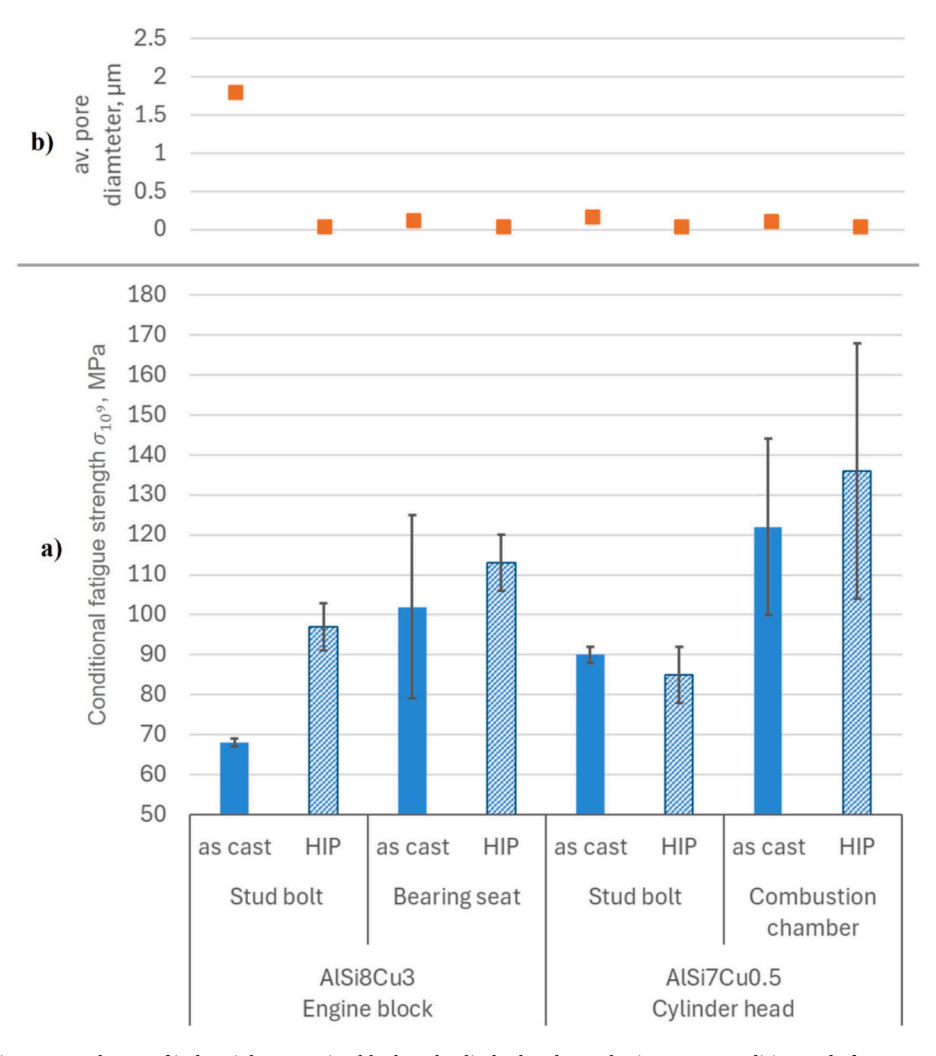


Fig. 16. a) Conditional fatigue strength  $\sigma_{10^{\circ}}$  of industrial cast engine block and cylinder head samples in as cast condition and after HIP treatment (ultrasonic fatigue testing at 20 kHz and R = -1, testing device UFTE from Boku Vienna) as well as b) corresponding average pore diameter.

### 3.5. Fatigue improvement by pore modification

The previous analyses have shown that pores have a massive influence on the fatigue life, especially in the case of large, fissured shrinkage pores or pores in near-surface regions. In addition to the reduced fatigue strength, the large scatter caused by the unpredictable formation of shrinkage pores in real components is also a massive problem. However, as shrinkage pores are often unavoidable in complex components, it is finally discussed whether the fatigue strength can be improved by the targeted modification of the pore size and morphology. Initial tests, which were carried out on the industrially relevant and extensively investigated alloy AlSi11Mg, show that gassing of the melt with hydrogen can specifically influence pore evolution. The as-cast state Fig. 19a) shows fissured shrinkage pores in the centre of the sample, whereas the entire sample volume is filled with small, spherical hydrogen pores as a result of hydrogen gassing (Fig. 19b). For experimental details please refer to previous publication [11].

By means of cyclic testing, extensively published as Wöhler S/N diagrams in [11], it was shown that small spherical hydrogen pores can significantly reduce the scattering of the service life and improve the predictability of the component performance. However, an increase in service life has not yet been achieved and requires better optimisation of the pore size and shape, which is the focus of ongoing future research work. The aim is to influence crack growth by optimising the size of the spherical pores. Crack propagation tests, which provide insights into the interaction between the crack tip and pores, already provide promising

results (Fig. 20). The as-cast condition shows a better threshold value for technical crack propagation of  $\Delta K_{th}=7.6$  MPa  $m^{0.5}$  compared to the ascast condition of  $\Delta K_{th}=6.2$  MPa  $m^{0.5}.$ 

However, it is particularly noteworthy that pores significantly slow down fatigue crack propagation, as the slope of the Paris line illustrates. Crack growth in hydrogen gassified samples is significantly lower (0.6 nm/load cycle• MPa m $^{0.5}$ ) compared to the as-cast state (5.4 nm/load cycle• MPa m $^{0.5}$ ) (cf. Fig. 21). The reason for this is a deflection of the crack tip due to the pores, as can be seen from the  $\mu\text{-CT}$  images. The three mechanisms i) crack deflection, ii) crack splitting and iii) crack tip blunting can thus lead to a slowdown in crack growth. The targeted utilisation of these mechanisms through pore engineering is the subject of further research activities.

#### 4. Conclusion

The fatigue behavior of cast Aluminium materials is characterized by a very inhomogeneous microstructure, especially in complex industrial components with locally varying cooling rates and solidification conditions. Based on various fatigue experiments and crack propagation tests on the primary alloy AlSi7Mg0.3 and the secondary alloy AlSi8Cu3, combined with microstructure analysis, the most important influencing factors were identified. In the industrially manufactured engine block and cylinder head, strong local deviations in the fatigue strength were observed, which are attributed microstructural heterogeneities, especially fraction and morphology of eutectic Si and intermetallics, SDAS,

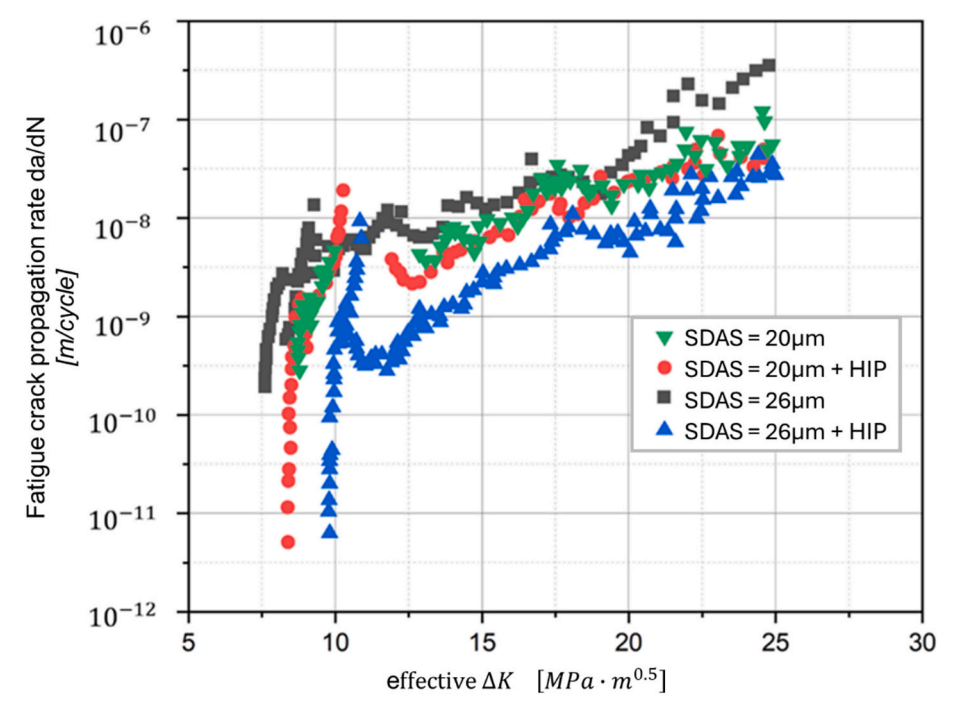


Fig. 17. Crack progression rate da/dN as a function of the effective  $\Delta K$  (stress intensity factor amplitude for R=-1) for the cylinder head made of AlSi7Cu0.5 Mg for different SDAS and HIP (bending resonance frequency testing at 100 Hz using single-edge notched bend (SENB) samples, R=-1).

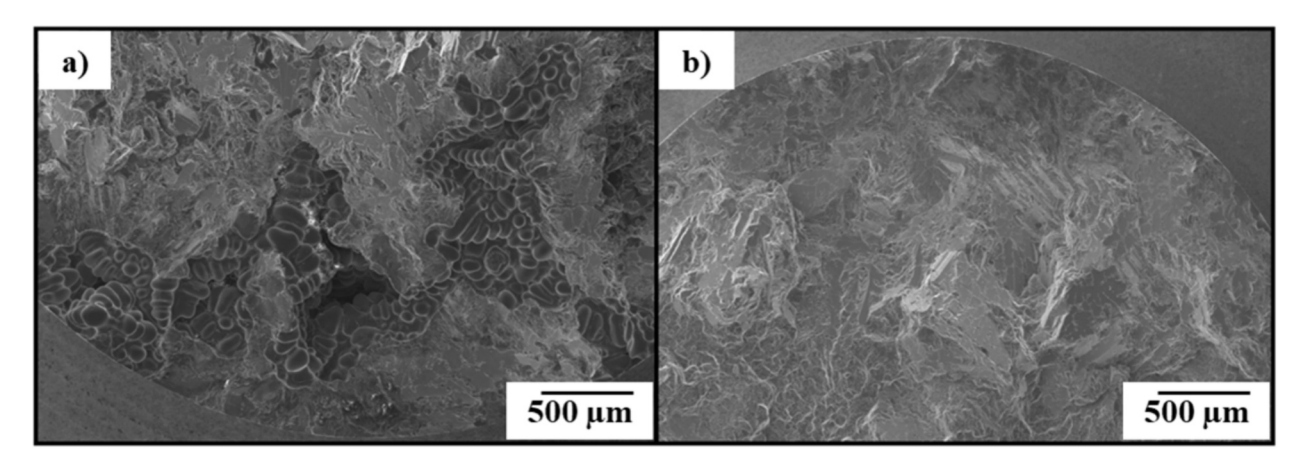


Fig. 18. Fracture surfaces from the wedge cast AlSi7Mg0.3 in a) SDAS =  $59 \mu m$ ,  $\sigma_a = 90 MPa$  and  $N_f = 1.01 \bullet 10^8$  cycles and b) SDAS =  $72 \mu m$ ,  $\sigma_a = 75 MPa$  and  $N_f = 3.84 \bullet 10^8$  cycles.  $\bullet$ .

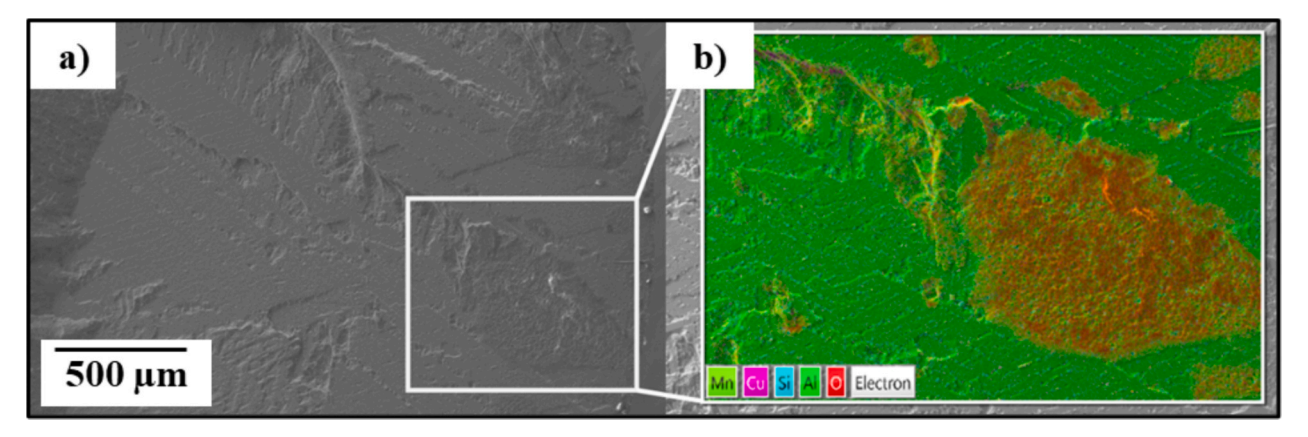


Fig. 19. AlSi8Cu3 alloy from engine block showing facet fracture surface with oxide inclusions; loaded with  $\sigma = 100$  MPa and  $N_f = 2.3 \bullet 10^8$  cycles. a) fracture surface and b) EDX analysis (shows partial oxide occupancy – red).

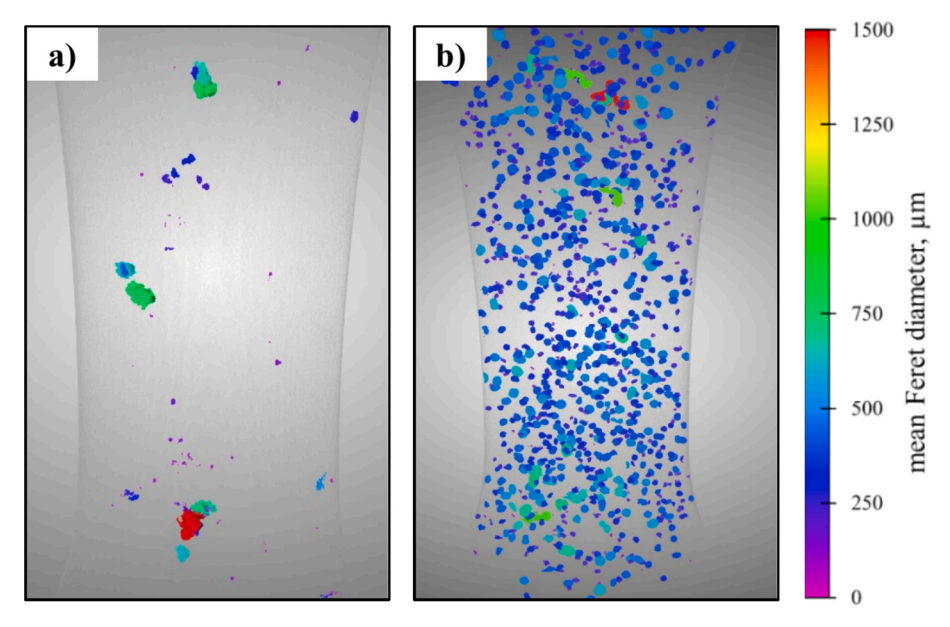


Fig. 20. Pore distribution of the fatigue samples prior to testing for a) conventional casting and b) pore modification by hydrogen upgassing of the melt. Colour code represents the mean Ferret diameter (maximum diameter of the pore circumference). The conventional casting shows large fissured shrinkage pores, whereas the gasified sample exhibits spherical pores which are homogeneously distributed [11].

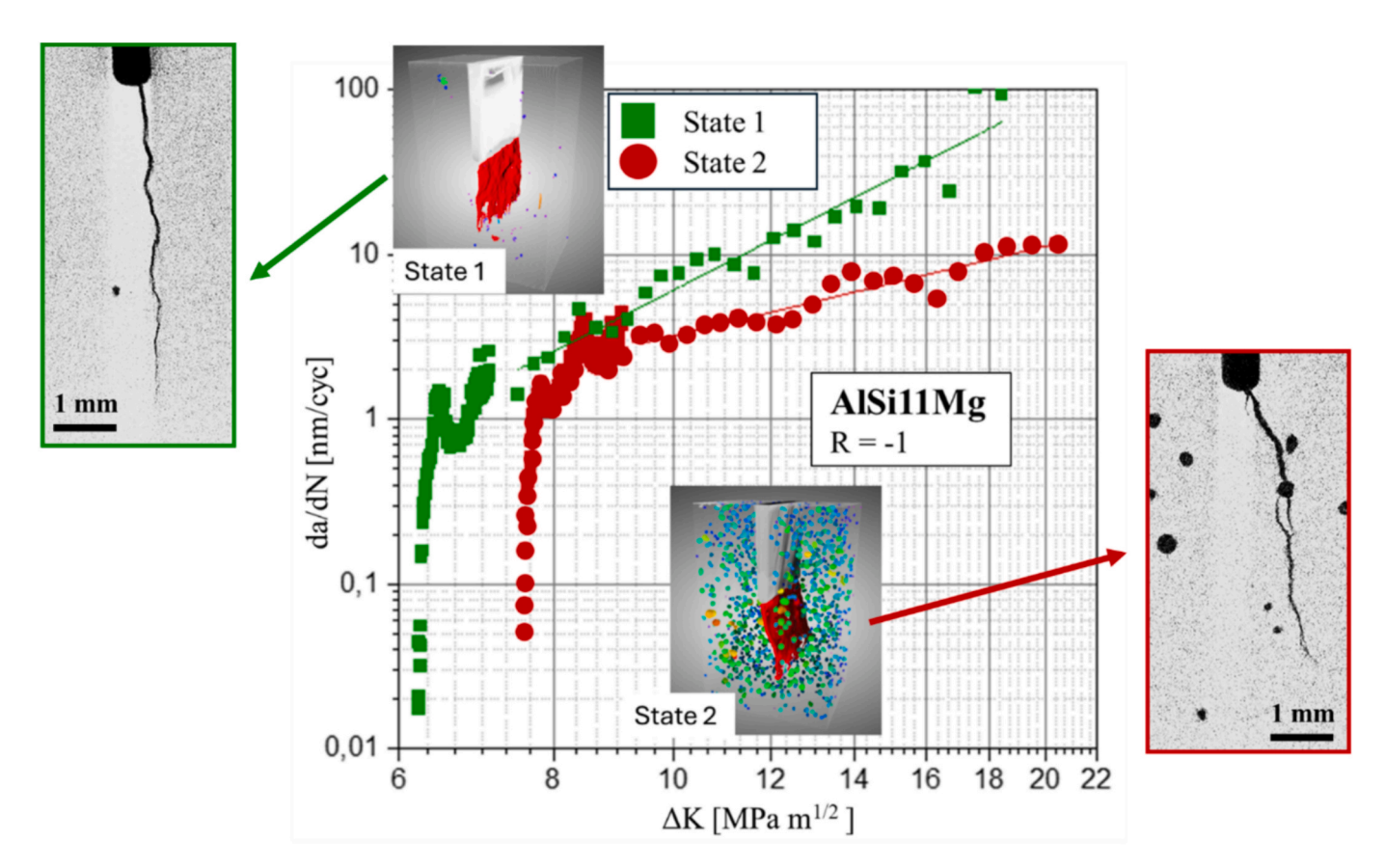


Fig. 21. Crack propagation curves of melt state 1 (conventional cast reference condition) and state 2 (pore modification by hydrogen upgassing); data obtained by bending resonance frequency testing at 100 Hz using single-edge notched bend (SENB) samples, R = -1 [11].

and pore fraction, size and shape. Since a higher SDAS is usually associated with a higher pore size and larger Si particles with a lower shape factor, the individual influencing factors were investigated in isolation using laboratory castings with defined variations in individual microstructural features. It was demonstrated that cracks propagate

preferentially and with high crack propagation rate in dendritic  $\alpha$ -Aluminium. At the interface to interdendritic eutectic silicon, cracks tend to be deflected, which can lead to a reduction of crack propagation rate. A lower SDAS and thus a higher fraction of interfaces is therefore advantageous, which is expressed in a higher fatigue, analogous to the

Hall Petch relationship. However, near-threshold crack growth resistance is improved by a higher SDAS, which is explain by higher roughness-induced crack closure effects.

Pores are another critical factor, with large, fissured shrinkage pores drastically reducing service life and leading to high scattering. Hydrogen gasification of the melt prior to casting can replace shrinkage pores with small spherical hydrogen pores, which can slow down the crack propagation rate through crack deflection, crack tip blunting and crack splitting.

To summarize, the VHCF strength and damage tolerance of cast Al alloys can be tailored by adjusting the local cooling conditions (low/high SDAS), heat treatment and pore modification. By controlling these microstructural features, it is possible to design cast Al alloys with improved fatigue performance and increased service life.

#### CRediT authorship contribution statement

M. Kreins: Writing – original draft, Visualization, Conceptualization. H. Kannan: Writing – original draft, Visualization. S. Scherbring: Writing – original draft, Methodology, Investigation, Data curation, Conceptualization. A. Bührig-Polaczek: Supervision, Funding acquisition. J. Tenkamp: Investigation, Data curation. F. Walther: Supervision, Funding acquisition. W. Michels: Supervision. U. Krupp: Writing – review & editing, Supervision, Funding acquisition, Conceptualization.

#### Declaration of competing interest

The authors declare that they have no known competing financial interests or personal relationships that could have appeared to influence the work reported in this paper.

# Acknowledgements

The research work was carried out within the framework of the AiF (German Federation of Industrial Research Associations e.V.) project 21018N, funded by the German Federal Ministry of Economics and Climate Protection (Bundesministerium für Wirtschaft und Klimaschutz) and by the German Ministry of Education and Research (BMBF, project number 13FH027PX5), as well as within the framework of the project no. 496240495 (WA 1672/101-1, KR 1999/50-1) funded by the German Research Foundation (Deutsche Forschungsgemeinschaft, DFG). The support by Nemak Dillingen GmbH and RWP GmbH is gratefully appreciated.

# Data availability

The raw/processed data required to reproduce the findings in the study cannot be shared at this time, as the data also forms part of several ongoing studies. However, the data may be made available from the corresponding author upon request.

#### References

- [1] Wang M, Song B, Wei Q, Zhang Y, Shi Y. Effects of annealing on the microstructure and mechanical properties of selective laser melted AlSi7Mg alloy. Mater Sci Eng: A 2019;739:463–72. https://doi.org/10.1016/j.msea.2018.10.047.
- [2] Siegfanz S, Giertler A, Michels W, Krupp U. Influence of the microstructure on the fatigue damage behaviour of the aluminium cast alloy AlSi7Mg0.3. Mater Sci Eng: A 2013;565:21–6. https://doi.org/10.1016/j.msea.2012.12.047.
- [3] Osmond P, Bellett D, Le VD, Morel F. Effect of over-ageing on the tensile and torsional fatigue properties of the AlSi7Cu0.5 Mg0.3 precipitation-hardened cast aluminium alloy. Int J Fatigue 2025;190:108615. https://doi.org/10.1016/j. iifatigue.2024.108615.
- [4] Gao T, Ji C, Zhan Z, Huang Y, Liu C, Hu W, et al. A novel defect-based fatigue damage model coupled with an optimized neural network for high-cycle fatigue analysis of casting alloys with surface defect. Int J Fatigue 2023;170:107538. https://doi.org/10.1016/j.ijfatigue.2023.107538.

- [5] Niu X, He C, Zhu SP, Foti P, Berto F, Wang L, et al. Defect sensitivity and fatigue design: deterministic and probabilistic aspects in AM metallic materials. Prog Chem Org Nat Prod Mater Sci 2024:101290. https://doi.org/10.1016/j. pmatsci 2024 101290
- [6] Hardin RA, Beckermann C. Prediction of the fatigue life of cast steel containing shrinkage porosity. Metall Mater Trans A 2009;40(3):581–97. https://doi.org/ 10.1007/s11661-008-9755-3
- [7] Tijani Y, Heinrietz A, Stets W, Voigt P. Detection and influence of shrinkage pores and nonmetallic inclusions on fatigue life of cast aluminum alloys. Metall Mater Trans A 2013;44(12):5408–15. https://doi.org/10.1007/s11661-013-1773-0.
- [8] Wang QG, Crepeau PN, Davidson CJ, Griffiths JR. Oxide films, pores and the fatigue lives of cast aluminum alloys. Metall Mater Trans B 2006;37(6):887–95. https://doi.org/10.1007/BF02735010.
- [9] Wang Q, Apelian D, Lados D. Fatigue behavior of A356-T6 aluminum cast alloys. Part I. Effect of casting defects. J Light Metals 2001;1(1):73–84. https://doi.org/ 10.1016/S1471-5317(00)00008-0
- [10] Gao YX, Yi JZ, Lee PD, Lindley TC. The effect of porosity on the fatigue life of cast aluminium-silicon alloys. Fatigue Fract Eng Mat Struct 2004;27(7):559–70. https://doi.org/10.1111/j.1460-2695.2004.00780.x.
- [11] Kreins M, Hippe M, Funken F, Phyu MP, Bührig-Polaczek A, Krupp U. Effect of shrinkage versus hydrogen pores on fatigue life of cast AlSi11Mg alloy. Inter Metalcast 2024. https://doi.org/10.1007/s40962-024-01288-7.
- [12] Blankenship CP, Hornbogen E, Starke EA. Predicting slip behavior in alloys containing shearable and strong particles. Mater Sci Eng: A 1993;169(1–2):33–41. https://doi.org/10.1016/0921-5093(93)90596-7.
- [13] Gerbe S, Krupp U, Michels W. Influence of secondary dendrite arm spacing (SDAS) on the fatigue properties of different conventional automotive aluminum cast alloys. Frattura ed Integrità Strutturale 2019;13(48):105–15. https://doi.org/10.3221/IGF-ESIS.48.13.
- [14] Raghavendra AKM, Maurel V, Marcin L, Proudhon H. Fatigue life prediction at mesoscopic scale of samples containing casting defects: A novel energy based nonlocal model. Int J Fatigue 2024;188:108485. https://doi.org/10.1016/j. iifatigue.2024.108485.
- [15] Liang Y, Zuo Z, Wang J, Zha C, Ren, Huang W. Study on high cycle fatigue behaviours and modelling of cast aluminium alloy at elevated temperatures. Eng Fail Anal 2025;168:109031. https://doi.org/10.1016/j.engfailanal.2024.109031.
- [16] Gerbe S, Knorre S, Krupp U, Michels W. The significance of microstructure heterogeneities on the fatigue thresholds of aluminum castings. MATEC Web Conf. 2018;165:14005. https://doi.org/10.1051/matecconf/201816514005.
- [17] VDG. Bestimmung des Dendritenarm- abstandes für Gussstücke aus Aluminium-Gusslegierungen: Bundesverband der deutschen Giesserei Industrie(P220): VDG Düsseldorf: 2011.
- [18] International Organization for Standardization. Metallic materials Fatigue testing — Axial force-controlled method;1099:2017(ISO 1099:2017(E)). Switzerland: ISO; 2017.
- [19] Deutsches Institut für Normung e. V. Schwingfestigkeitsversuch Durchführung und Auswertung von zyklischen Versuchen mit konstanter Lastamplitude für metallische Werkstoffproben und Bauteile;19.060; 77.040.10(DIN 50100:2022-12). Berlin: Beuth Verlag GmbH; 2022.
- [20] Hück M. Ein verbessertes Verfahren für die Auswertung von Treppenstufenversuchen. Materialwissenschaft und Werkstofftechnik 1983;14(12): 406–17. https://doi.org/10.1002/mawe.19830141207.
- [21] E08 Committee. Test method for measurement of fatigue crack growth rates. West Conshohocken, PA: ASTM International. DOI: 10.1520/E0647-24.
- [22] Paris P, Erdogan F. A Critical analysis of crack propagation laws. J Basic Eng 1963; 85(4):528–33. https://doi.org/10.1115/1.3656900.
- [23] El Haddad MH, Smith KN, Topper TH. Fatigue crack propagation of short cracks. J Eng Mater Technol 1979;101(1):42-6. https://doi.org/10.1115/1.3443647.
- [24] Krupp U. Fatigue crack propagation in metals and alloys: microstructural aspects and modelling concepts. John Wiley & Sons 2007. https://doi.org/10.1002/ 9783527610686.
- [25] Pramod SL, Ravikirana RAP, Murty BS, Bakshi SR. Effect of Sc addition and T6 aging treatment on the microstructure modification and mechanical properties of A356 alloy. Mater Sci Eng: A 2016;674:438–50. https://doi.org/10.1016/j.msea.2016.08.022.
- [26] Stadler F, Antrekowitsch H, Fragner W, Kaufmann H, Uggowitzer PJ. Effect of main alloying elements on strength of Al–Si foundry alloys at elevated temperatures. Int J Cast Metals Res 2012;25(4):215–24. https://doi.org/10.1179/ 1743133612Y.0000000004.
- [27] Trudonoshyn O, Prach O, Slyudova A, Lisovskii V. Structure formation and multistep nucleation in casting Al-Mg-Si alloys. Int J Cast Metals Res 2020;33(4–5): 184–93. https://doi.org/10.1080/13640461.2020.1822632.
- [28] Yi JZ, Gao YX, Lee PD, Lindley TC. Microstructure-based fatigue life prediction for cast A356-T6 aluminum-silicon alloys. Metall Mater Trans B 2006;37(2):301–11. https://doi.org/10.1007/BF02693159.
- [29] Yajjala RK, Inampudi NM, Jinugu BR. Correlation between SDAS and mechanical properties of Al–Si alloy made in sand and slag moulds. J Mater Res Technol 2020; 9(3):6257–67. https://doi.org/10.1016/j.jmrt.2020.02.066.
- [30] Yan K, Huang W, Zuo Z, Ren P, Li D, Zhao C, et al. Microstructure based analysis and predictive modeling of cast Al7Si1.5Cu0.4Mg alloy mechanical properties. Mater Today Commun 2022;30:103102. https://doi.org/10.1016/j. mtcomm.2021.103102.
- [31] Chapetti M, Miyata H, Tagawa T, Miyata T, Fujioka M. Fatigue strength of ultrafine grained steels. Mater Sci Eng: A 2004;381(1–2):331–6. https://doi.org/ 10.1016/j.msea.2004.04.055.

- [32] Lang Y, Ci X, Qiao H, Ma X, Wang W, Kong D, et al. Evaluation of fatigue behavior of a casting aluminum knuckle considering influences of inhomogeneous microstructure. Eng Fail Anal 2025;168:109102. https://doi.org/10.1016/j. engfailanal.2024.109102.
- [33] Lados DA. Fatigue crack growth mechanisms in Al-Si-Mg alloys. Surf Eng 2004;20 (6):416-24. https://doi.org/10.1179/sur.2004.20.6.416.
- [34] Moustafa MA. Effect of iron content on the formation of β-Al5FeSi and porosity in Al-Si eutectic alloys. J Mater Process Technol 2009;209(1):605–10. https://doi. org/10.1016/j.jmatprotec.2008.02.073.
- [35] Nayhumwa C, Green NR, Campbell J. Influence of casting technique and hot isostatic pressing on the fatigue of an Al-7Si-Mg alloy. Metall Mater Trans A 2001; 32(2):349–58. https://doi.org/10.1007/s11661-001-0266-8
- 32(2):349–58. https://doi.org/10.1007/s11661-001-0266-8.

  [36] Wang Q, Apelian D, Lados D. Fatigue behavior of A356/357 aluminum cast alloys. Part II Effect of microstructural constituents. J Light Metals 2001;1(1):85–97. https://doi.org/10.1016/S1471-5317(00)00009-2.
- [37] Campbell J. An overview of the effects of bifilms on the structure and properties of cast alloys. Metall Mater Trans B 2006;37(6):857–63. https://doi.org/10.1007/ BF02735006.